Achromatic Broadband Super-Resolution Imaging by Super-Oscillatory Metasurface

Zhu Li, Tao Zhang, Yanqin Wang, Weijie Kong, Jian Zhang, Yijia Huang, Changtao Wang, Xiong Li, Mingbo Pu, and Xiangang Luo*

Past decades have seen enormous efforts to achieve subdiffraction resolution optical imaging, but most of them are suffering from either complex near-field manipulation or prelabeling of specific specimen, like scanning near-field optical microscopes and stimulated emission depletion microscopes. The optical super-oscillation phenomenon seems to provide a method of far field super-resolution imaging without particularly dealing with objects. However, the reported optical super-oscillation imaging methods were usually constrained to narrow bandwidth, which is mainly due to the inherent complex light interference features. Here, benefiting from the nearly dispersionless feature of phase modulations with metasurface, a super-oscillatory metasurface filter is proposed for broadband super-resolution imaging. In demonstrative experiments, resolving ability of about 0.64 times of the Rayleigh criterion is obtained for visible light ranging from 400 to 700 nm. This method is expected to potentially promote the development of super-resolving telescopes and microscopes based on super-oscillation optics.

1. Introduction

It is well known that the resolution of optical system is dependent on the wavelength of the illuminating light and the effective numerical aperture (NA), as defined by the Rayleigh criterion.[1] Consequently, intensive efforts have been made to break this

Dr. Z. Li, Dr. T. Zhang, Prof. Y. Wang, Prof. W. Kong, Prof. J. Zhang,
Dr. Y. Huang, Prof. C. Wang, Prof. X. Li, Prof. M. Pu, Prof. X. Luo
State Key Laboratory of Optical Technologies on Nano-Fabrication and
Micro-Engineering
Institute of Optics and Electronics
Chinese Academy of Sciences
Chengdu 610209, China
E-mail: lxg@ioe.ac.cn
Dr. T. Zhang
Key Laboratory of Opto-electronic Technology and Systems of the
Education Ministry of China
Chongqing University
Chongqing 400044, China
Dr. Z. Li, Dr. T. Zhang, Dr. Y. Huang
University of Chinese Academy of Sciences
Beijing 100049, China

The ORCID identification number(s) for the author(s) of this article
can be found under https://doi.org/10.1002/lpor.201800064

barrier for centuries, such as the scanning near-field optical microscopy (SNOM),[2] superlens,[3] and hyperlens,[4] by exploiting the evanescent wave containing fine details of objects.[5] These methods allow subdiffraction imaging at the cost of complex near-field operation. Besides, some super-resolution microscopes with manipulations of fluorescence radiation, including photo-activated localization microscope (PALM)[6] and stimulated emission depletion (STED),[7] deliver impressive achievement in obtaining nano-features of bio-samples. Due to the prelabeling of samples by specific dyes, however, it has limited applications. Therefore, it would be imperative to have an access for far-field noninvasive super-resolution imaging.

In 1952, Toraldo[8] proposed the super-gain antenna in microwave and optics to improve the resolution of imaging in the far field, which is regarded as a well-known pupil-filtering technology,[9] and made extensive applications in beam shaping.[10] More recently, the super-oscillation phenomenon was put forward by Berry and Popescu.[11] They found that the super-oscillation behavior occurs in a region where the band-limited functions are able to oscillate faster than their highest Fourier components, which is somewhat similar to the weak measurements in quantum mechanics,[12] and this phenomenon usually arises from complex destructive interference of light with different spatial frequencies and variant phases. Based on the super-oscillation interference, super-oscillation lens (SOL) provides an unprecedented avenue for far-field noninvasive super-resolution imaging, as demonstrated in experiments.[13] SOL has been successfully applied to the subdiffraction focusing and imaging[14–17] as well as the heat assisted magnetic recording in confocal scanning system.[18] The key point of super-oscillation imaging is appropriate pupil filter in imaging optics, which is usually realized by binary amplitude elements,[13] spatial light modulators[19] or specially designed nanostructures.[20] Unfortunately, this would inevitably render great variance of phase modulation for variant light wavelengths. In 2015, an ultrabroadband super-oscillatory lens (UBSOL)[21] has been proposed and experimentally verified to achieve subwavelength focusing behavior for wavelengths over the whole visible and near-infrared light. However, it is confronted with the problem of axial chromatic dispersion. Recently,
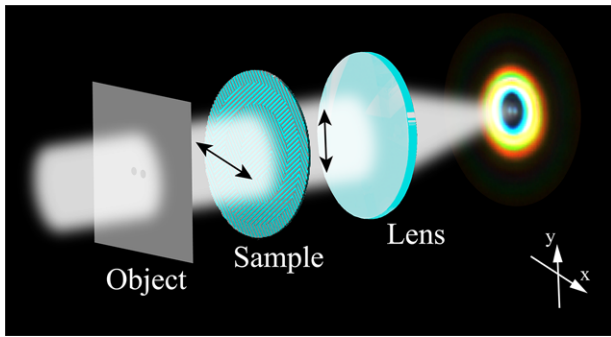
ADVANCED
SCIENCE NEWS

www.advancedsciencenews.com

www.lpr-journal.org

LASER
& PHOTONICS
REVIEWS

Figure 1. Schematic of achromatic broadband super-resolution imaging by super-oscillatory metasurface.

the achromatic super-oscillatory lenses have realized the sub-wavelength focusing,[22] but it could only work in several designed wavelengths. As a result, the SOLs still face the trouble of narrow working bandwidth, which limits its feasibility to some special applications.

In this article, a white-light super-oscillation imaging system is proposed by using the dispersionless spin–orbit interaction[23] in geometric metasurfaces,[24,25] which provides perfect 0 and π phase-only manipulation for the white light. This unique property of metasurface avoids great chromatic phase aberration in conventional optics and helps to generate broadband super-oscillation imaging feature. As a proof of concept, super-oscillatory imaging patterns of extended targets have been successfully obtained for visible light ranging from 400 to 700 nm and the subdiffraction resolution is about 0.64 times of the Rayleigh limitation.

2. Design of Metasurface Filter

As illustrated in **Figure 1**, the metasurface filter is positioned at the exit-pupil plane of the imaging optical system, and objects illuminated with white incoherent light could be imaged at the image plane away from the metasurface filter. For the simplicity of analysis, the image performance could be regarded as an achromatic lens combined with the metasurface filter with phase function $\varphi_{MF}(r)$, and the point spread function (PSF) of the system could be depicted as[26]

$$I(\rho) \propto \left(\frac{1}{\lambda f}\right)^2 \left| \int_0^R \exp[i\varphi_{MF}(r)] J_0\left(\frac{2\pi r\rho}{\lambda f}\right) r\, dr \right|^2 \quad (1)$$

Here λ is the light wavelength, f is the focal length of the achromatic lens, and R is the aperture radius of the metasurface. The aim of designing metasurface filter with specific phase-change positions is to yield a PSF with minimum width of main lobe and small side lobe levels within the local field of view (FOV). This step could be performed by optimization methods[27] like linear programming methods,[28] or particle swarm optimization.[29] In this way, a super-oscillatory PSF pattern is finally attained on the imaging plane.

The key point of the metasurface filter (MF) method is the employment of metasurface composed of nanoscale gratings with
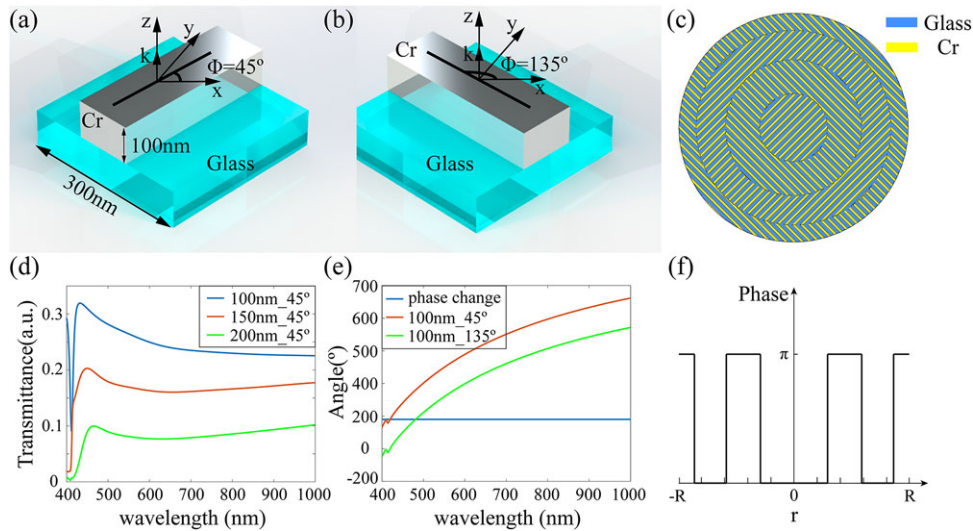
variant orientations in concentric ring regions. Instead of using phase retardations in conventional binary micro structures etched on transparent substrates or spatial light modulators, the phase modulation of MF arises from the Pancharatnam–Berry phase, or so-called photonic spin–orbit interaction in structures such as rotating dipoles and optical catenaries.[30,31] This occurs as light in certain polarization state transmits through the nanograting structure and will be partly converted to the crossed polarization with phase variation dependent on the orientations of nanograting with respect to the incident light polarization. Thus the transmitted light of cross-polarization possesses a specific geometric phase profile, which exhibits a nearly dispersionless feature in broadband spectrum. The transmission efficiency is related to the width and period of the grating, which can be described by a catenary-like impedance dispersion curve.[32] As we will discuss elsewhere, the catenary dispersion, catenary structures, and catenary optical fields form the bases for the catenary optics.[30]

As a demonstrative example, a metasurface structure is designed to contain arrays of customized rectangular metallic gratings with $\varphi = 45°$ and $\varphi = 135°$ etched on a glass substrate, where φ is the angle between axis x and the orientation of the grating. The rectangular nanometallic gratings with two orthogonal orientations, 300 nm × 300 nm period, and 100 nm thickness are shown in **Figure 2**a,b. Since the efficiency of the unit cell usually has a strong dependence on the width of the grating theoretically, the light-field manipulation ability of the unit cells with the width of 100, 150, and 200 nm are simulated by the commercial software CST Microwave Studio, respectively. For simplicity of fabrication, the chromium (Cr) is used as the grating material. As illustrated in Figure 2d, the Cr grating with the width of 100 nm is finally chosen to achieve higher energy efficiency in a broad spectrum from 400 to 1000 nm. Furthermore, the modulated phase change of the transmitted light field is approximately fixed to 180 ° in broadband as illustrated in Figure 2e. In principle, the geometric phase is inherently dispersionless as reported in previous research.[21] In view of the convenience of fabrication, the binary phase modulations are adopted in the metasurface filter.

In Figure 2c,f, the metasurface is designed to contain four regions with the normalized radius of each phase-jump position $r_1 = 0.297$, $r_2 = 0.594$, and $r_3 = 0.85$, and these parameters have been demonstrated to obtain a 0.6 times the full width of Airy pattern in theory. For such a unique metasurface, the unit cells in Figure 2a,b are distributed alternately in neighboring annuli. As the orientations of the units in neighboring circles are orthogonal with each other, following the Pancharatnam–Berry phase, the metasurface could successfully provide nearly perfect 0 and π dispersionless phase manipulation for the incident white light. In the local coordinates,[30] the transmission and reflection property can be described by the generalized Fresnel's equations:[23]

$$r_{u,v} = \frac{Y_1 - Y_2 - Y_{u,v}}{Y_1 + Y_2 + Y_{u,v}}, \quad t_{u,v} = \frac{2Y_1}{Y_1 + Y_2 + Y_{u,v}} \quad (2)$$

where Y_1 and Y_2 are the admittance of the materials at the two sides, and $Y_{u,v}$ is the anisotropic admittance of the metasurface.

ADVANCED
SCIENCE NEWS

www.advancedsciencenews.com

LASER
& PHOTONICS
REVIEWS

www.lpr-journal.org

Figure 2. Schematic of the unit cell with a) $\varphi = 45°$ and b) $\varphi = 135°$. c) Structure of the metasurface whose diameter is 9 mm. d) Transmission efficiency of the unit cells with different widths of Cr. e) Phase shift of unit cell with different orientations. f) Radial phase distribution of metasurface.
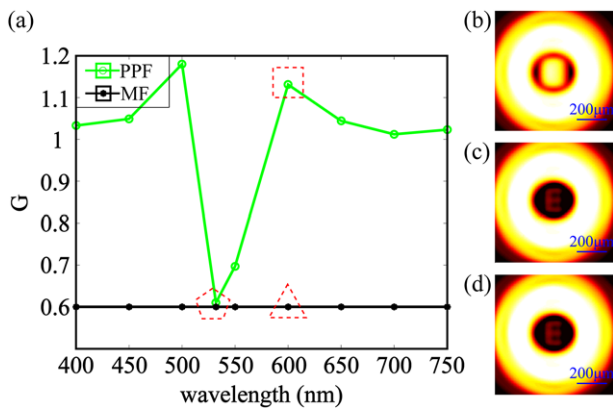
Figure 3. a) Comparison of G distribution between PPF and MF as the wavelengths range from 400 to 750 nm. b–d) simulation results for imaging of "E," corresponding wavelength points in square, triangle, and pentagon, respectively. "E" is selected to be 100 μm × 124 μm.

3. Comparison of Imaging with Metasurface, Binary Phase Pupil Filters

The unique dispersionless phase-only manipulation property of the metasurface for white light plays a significant role in the broadband super-oscillation imaging. Based on the pupil filtering technique, the 0-π phase annular pupil filter (PPF)[33] could realize the super-resolution imaging. To show the advantage of metasurface filter, the comparison of these two super-oscillation imaging performances is presented below.

By combining the linear optimization algorithm, the PPF and the MF are designed to work on a resolvable ability to 0.6 times of Rayleigh criterion (assuming λ is 532 nm, R is 4.5 mm, and f is 500 mm), with the normalized radius of each phase-jump position $r_1 = 0.297$, $r_2 = 0.594$, and $r_3 = 0.85$. **Figure 3**a shows the resolution factor G of these two methods for light wavelength ranging from 400 to 750 nm. Obviously, the PSF width of PPF method

shows strong dependence on the light wavelength, where the super-oscillation effect occurs closely at the working wavelength 532 nm and G increases greatly as wavelength goes slightly away from it. This phenomenon indicates that super-oscillation is sensitive to the change of phase modulation, even for 10% variance generated by a binary phase structure with about 50 nm wavelength deviation,[30]

$$\frac{2\pi}{\lambda} \Delta d(n - 1) = \pi \tag{3}$$

where Δd and n means the etched depth and refraction index of the glass, which are about 578 nm and 1.46 here.

From Equation (3), apparently, the super-resolving ability of PPF significantly relies on the wavelengths, and therefore the PPF can only be applied to the imaging within a narrow bandwidth. This point demonstrates clearly that the super-oscillation phenomenon exhibits great fragility to the slight change of light fields, as it arises from the delicate light interference behaviors. This can be further demonstrated by the simulation images of 'E' object in Figure 3b,c.

For the MF proposed in this article, due to its dispersionless phase manipulation behavior, it successfully overcomes the wavelength dependence feature of PPF as shown in Figure 3. As observed, the images of "E" in Figure 3c,d could be resolved clearly and the images have approximately the same imaging quality and contrast for both wavelengths at 600 and 532 nm. It is worth noting that the resolution enhancement factor G is scaled with the Airy spot size with correspondent light wavelength. Thus, the resolving ability would scale linearly with wavelength and the resolution of a MF imaging system is a sum result for a wide light wavelength range, which could be approximately equal to the central wavelength. On the other hand, it is believed that an arbitrary high resolution would be theoretically possible for MF if the negative issues like fabrication challenges, ultra-low energy efficiency could be relieved. From these points of view, MF could significantly promote the development of the broadband
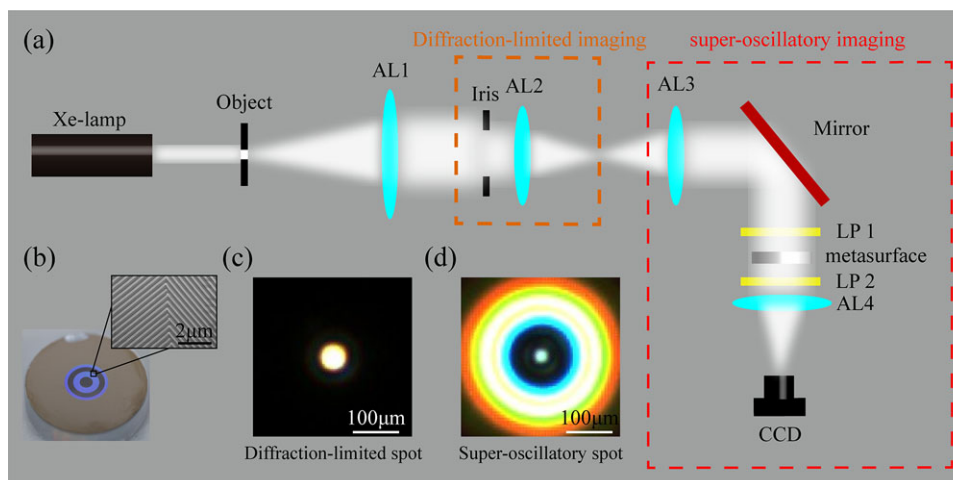
Figure 4. a) Schematic of experimental setup, including a Xe-lamp, an optical collimator (AL1, f = 1000 mm), an iris, three same achromatic lenses (AL2, AL3, AL4, f = 500 mm), a mirror, two linear polarizers (LP1, LP2), a designed metasurface, and a CCD (ICL-B2520C). b) The proposed metasurface. The inset indicates the distribution of the Cr gratings between two annuli. c) Diffraction-limited image of a hole with a diameter of 20 μm. d) Super-oscillatory image of a hole with a diameter of 20 μm. AL, achromatic lens. Here the positions and distances of elements are not in accurate scale with the experiment optic setup for a good visualization.

super-resolution imaging and could be applied to the imaging of microscope or telescope especially with interest of wide range of light wavelength.

4. Experimental Section

The experimental setup is mainly constituted of a diffraction-limited imaging section and a super-resolution imaging section. The object, illuminated by a white light source of Xe-lamp, is placed at the front focal plane of optical collimator (AL1), acting as the infinite distant target. First, it is imaged at the focal plane of lens (AL2) with finite aperture and the image here is diffraction limited. Following it is the relayed super-oscillatory imaging section, composed of a 4f system with two lenses: AL3 and AL4. At the exit pupil of the system, near the lens AL4, a pupil filter group is positioned with a specially designed metasurface filter sandwiched between two linear polarizers in crossed manner. The super-oscillatory image is recorded in the CCD at the second imaging plane.

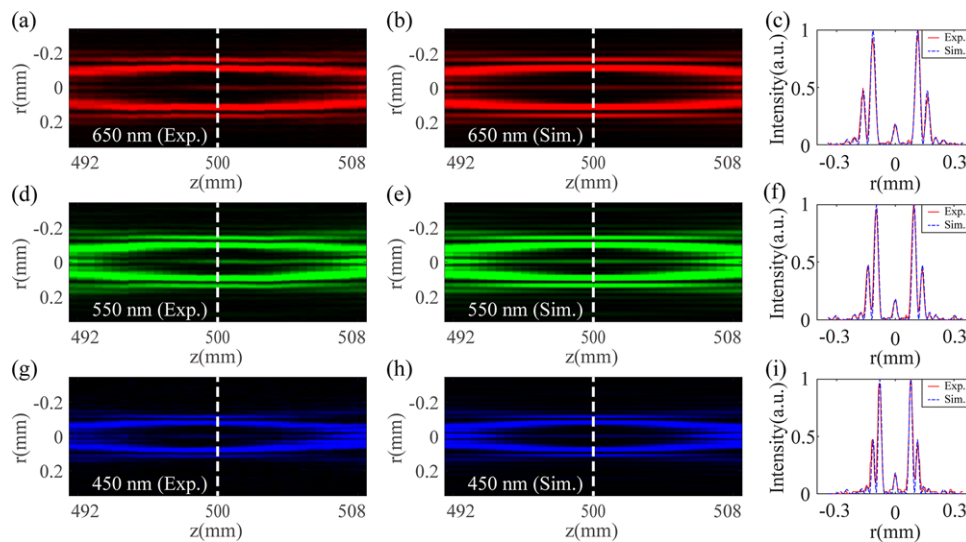## 5. Results and Discussions

5.1. PSF Measurement

First, the PSF is measured in the experiment by using a 20 μm diameter transparent circular hole on an opaque screen. For the case without the filter group, the measured PSF at CCD plane is an Airy spot with full width of 82.8 μm, as shown in **Figure 4**c. As the filter group is inserted in the optical setup, the PSF in Figure 4d exhibits an obvious super-oscillation PSF pattern with a much smaller bright central spot surrounded by a wide lobe ring pattern about few spot size away and with much higher brightness. The super-oscillation central spot size is about 51.75 μm, being 0.625 times of the Airy spot and slight larger than the de-

sign result $G = 0.6$ due to some inevitable errors like fabrication and aberration in optics. The central spot with reduced width provides the super-resolution imaging power of objects located inside the great lobe ring region of the super-oscillation PSF.

To precisely evaluate the PSF performance in experiment, three monochromatic light performances for the wavelengths of 650 ± 20, 550 ± 20, and 450 ± 20 nm are measured in variant image planes and compared with simulation results. As shown in **Figure 5**, the measured and simulated axial PSFs show nearly identical profiles, which demonstrate the good achromatic ability of the method proposed in this article, and the PSFs in the focal plane are also confirmed in the plots along the radial direction in the third column, in spite of some slight discrepancy of the small side lobes. In addition, we could see some edge position difference of the great side lobe rings for the three wavelengths. This helps to understand the colorful the ring pattern observed of the super-oscillation PSF in Figure 4d.

5.2. System Resolution Measurement

Further experimental imaging results in **Figure 6** are presented with two transparent holes with 20 μm diameter and 60 μm center-to-center distance beyond diffraction limited resolving power to demonstrate the resolving ability of the MF. As expected, the two point objects are totally unresolved for the case without MF (Figure 6a), and are clearly distinguished with MF (Figure 6b). The cross-sectional profiles of the two images are plotted in Figure 6c, showing the super-oscillatory image of the clearly resolved holes. Figure 6d plots the contrast of measured images for two holes with different center-to-center distances ranging from 20 to 120 μm. By assuming the resolving contrast criterion of about 0.153, the measured results show that the minimal resolvable distance of the two holes is about 60 μm and the minimal resolving ability is demonstrated to be approximately 0.64 times of Airy pattern.

ADVANCED
SCIENCE NEWS

www.advancedsciencenews.com

LASER
& PHOTONICS
REVIEWS

www.lpr-journal.org

Figure 5. a,d,g) Measured axial PSF at 650 ± 20, 550 ± 20, and 450 ± 20 nm. b,e,h) Simulated axial PSF with fixed wavelength of 650, 550, and 450 nm. c,f,i) Normalized PSF profiles along the radial direction in the focal plane of the theoretical and experimental results.
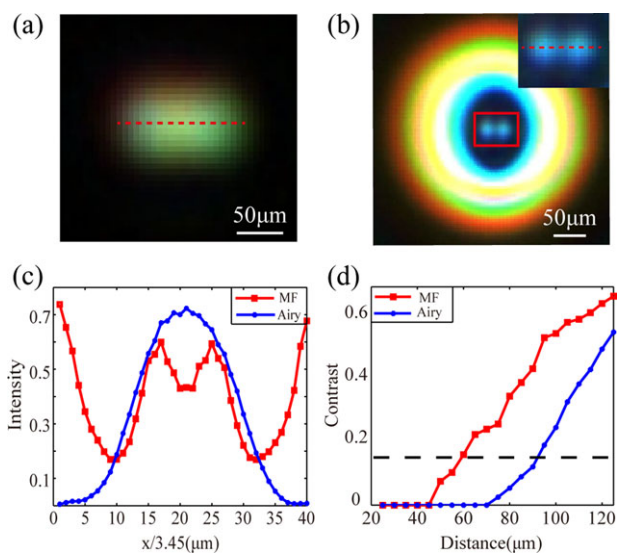
Figure 6. a) Diffraction-limited image. b) Super-oscillatory image. c) Intensity distribution of the central place marked by dashed lines in (a) and the insert of (b). d) Experiment imaging contrast for variant center-to-center distances of two-hole target. The dashed line is the contrast of Rayleigh criterion. Here the contrast is defined as $(Ip - Iv)/(Ip + Iv)$, where Ip is the peak intensity and Iv the central valley intensity. When the two point objects are unresolved, Ip is equal to Iv.

5.3. Extended Targets Imaging

The super-oscillation imaging also holds its super-resolution ability for extended objects as demonstrated in **Figure 7**. In this case, a target object "E" with 55 μm center-to-center and 100 μm width is used in our work (Figure 7a). Figure 7b shows that the "E" could not be resolved by the diffraction-limited imaging system, as predicted by the Rayleigh criterion. By employing MF, it could be imaged and resolved perfectly in Figure 7c. The comparison of intensity distribution between the diffraction-
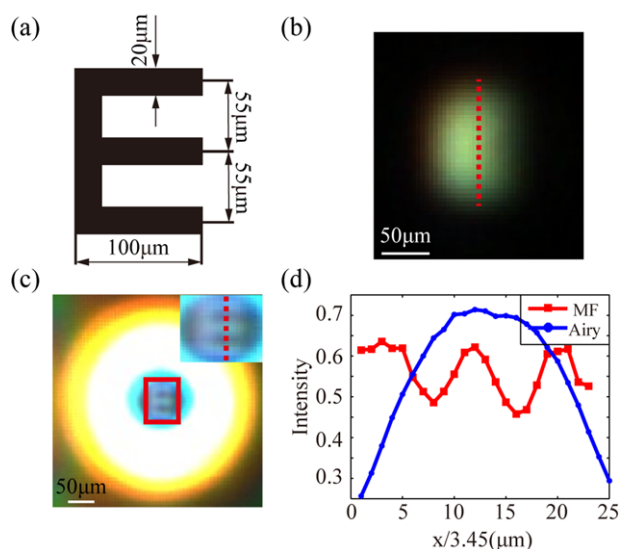
Figure 7. a) Target object "E." b) Diffraction-limited imaging of "E." c) Super-resolution imaging of "E." d) Intensity distribution of the place labeled by red dashed lines in (b) and the insert of (c).

limited pattern and the super-resolution one along the red line further verifies the super-resolving ability of MF in Figure 7d. It is obvious in Figure 7c that the image of "E" is surrounded by the high-intensity sidebands, which is the typical feature of the super-oscillation phenomenon. Besides, compared to ref. [22], our method could realize the subdiffraction imaging in the whole visible light, instead of several given wavelengths.

In principle, there always exist inevitable side lobes around the subdiffraction hotspot in the super-oscillation phenomenon, which are detrimental to imaging and render low efficiency and limited FOV. This phenomenon is also demonstrated in our experiments. Fortunately, it is the subdiffraction imaging feature in the far field that we are mainly concerned about. On the

one hand, the influence of limited FOV could be acceptable. According to the constraints on PSF, the special super-oscillatory pupil filter could be designed to make the FOV of PSF large enough so that the target objects are within the FOV. However, the efficiency would become lower with the increase of FOV. To solve the problem, some other methods have been used in super-oscillatory imaging, such as confocal scanning imaging,[13] stitched imaging.[26] On the other hand, the low efficiency may be tolerable for some specific applications, such as observing target object with high intensity. Besides, high-sensitivity detectors and long exposing time are also advantageous. Moreover, benefiting from the dispersionless phase modulations of metasurface filter, the light of the whole visible waveband could be utilized in our method, which relieves the demand on detection to some extent.

6. Conclusion and Outlook

In conclusion, a white-light super-oscillatory imaging system based on the metasurface filter is proposed and experimentally demonstrated. Benefiting from the specific geometric phase modulation independent of wavelength, the metasurface filter could be employed for super-resolution imaging over a wide range of light wavelength, circumventing the monochromatic restriction of super-oscillatory imaging with conventional phase plates. In addition, a resolution as high as 0.64 times that of Rayleigh criterion is observed in experiment with a white light source. It also holds its subdiffraction imaging ability for extended targets located inside super-oscillatory pattern region. It is believed that such MF provides an access for far-field and white-light super-oscillation imaging, which has potential promising applications in microscopes and telescope optics for bio imaging, astronomy observation, surveillance, and optical metrics. As a final remark, the super-oscillation phenomenon can be regarded as one anomalous interference effect, which is different from the near-field subwavelength interference known as "extraordinary Young's interference."[25,34]

Conflict of Interest

The authors declare no conflict of interest.

Keywords

broadband, metasurface, super-oscillation, super-resolution

[1] L. Rayleigh, *J. Roy. Micro. Soc.* **2011**, *23*, 474.
[2] E. Betzig, J. K. Trautman, T. D. Harris, J. S. Weiner, R. L. Kostelak, *Science* **1991**, *251*, 1468.
[3] J. B. Pendry, *Phys. Rev. Lett.* **2000**, *85*, 3966.
[4] Z. Jacob, L. V. Alekseyev, E. Narimanov, *Opt. Express.* **2006**, *14*, 8247.
[5] T. F. R. Edward, I. Z. Nikolay, *J. Opt.* **2013**, *15*, 094008.
[6] E. Betzig, G. H. Patterson, R. Sougrat, O. W. Lindwasser, S. Olenych, J. S. Bonifacino, M. W. Davidson, J. Lippincott-Schwartz, H. F. Hess, *Science* **2006**, *313*, 1642.
[7] S. W. Hell, J. Wichmann, *Opt. Lett.* **1994**, *19*, 780.
[8] G. T. Di Francia, *Nuovo Cimento* **1952**, *9*, 438.
[9] M. Martínez-Corral, P. Andrés, C. J. Zapata-Rodríguez, M. Kowalczyk, *Opt. Commun.* **1999**, *165*, 267.
[10] C. Ibáñez-López, L. Muñoz-Escrivá, G. Saavedra, M. Martínez-Corral, *Opt. Commun.* **2007**, *272*, 197–204.
[11] M. V. Berry, S. Popescu, *J. Phys. A: Math. Gen.* **2006**, *39*, 6965.
[12] Y. Aharonov, D. Z. Albert, L. Vaidman, *Phys. Rev. Lett.* **1988**, *60*, 1351.
[13] E. T. F. Rogers, J. Lindberg, T. Roy, S. Savo, J. E. Chad, M. R. Dennis, N. I. Zheludev, *Nat. Mater.* **2012**, *11*, 432.
[14] C. Hao, Z. Nie, H. Ye, H. Li, Y. Luo, R. Feng, X. Yu, F. Wen, Y. Zhang, C. Yu, J. Teng, B. Luk'yanchuk, C.-W. Qiu, *Sci. Adv.* **2017**, *3*, e1701398.
[15] F. Qin, K. Huang, J. Wu, J. Teng, C. W. Qiu, M. Hong, *Adv. Mater.* **2017**, *29*, 1602721.
[16] Y. Eliezer, L. Hareli, L. Lobachinsky, S. Froim, A. Bahabad, *Phys. Rev. Lett.* **2017**, *119*, 043903.
[17] T. Zacharias, B. Hadad, A. Bahabad, Y. Eliezer, *Opt. Lett.* **2017**, *42*, 3205.
[18] G. Yuan, E. T. F. Rogers, T. Roy, Z. Shen, N. I. Zheludev, *Opt. Express.* **2014**, *22*, 6428.
[19] A. M. H. Wong, G. V. Eleftheriades, *Sci. Rep.* **2013**, *3*, 1715.
[20] F. M. Huang, T. S. Kao, V. A. Fedotov, Y. Chen, N. I. Zheludev, *Nano Lett.* **2008**, *8*, 2469.
[21] D. Tang, C. Wang, Z. Zhao, Y. Wang, M. Pu, X. Li, P. Gao, X. Luo, *Laser Photon. Rev.* **2015**, *9*, 713.
[22] G. H. Yuan, E. T. F. Rogers, N. I. Zheludev, *Light Sci. Appl.* **2017**, *6*, e17036.
[23] X. Luo, *Sci. China-Phys. Mech. Astron.* **2015**, *58*, 594201.
[24] L. Zhang, S. Mei, K. Huang, C. W. Qiu, *Adv. Opt. Mater.* **2016**, *4*, 818.
[25] X. Luo, *Adv. Opt. Mater.* **2018**, *6*, 1701201.
[26] C. Wang, D. Tang, Y. Wang, Z. Zhao, J. Wang, M. Pu, Y. Zhang, W. Yan, P. Gao, X. Luo, *Sci. Rep.* **2015**, *5*, 18485.
[27] E. Katzav, M. Schwartz, *IEEE Trans. Signal Process.* **2013**, *61*, 3113.
[28] H. Liu, Y. Yan, Q. Tan, G. Jin, *J. Opt. Soc. Am. A.* **2002**, *19*, 2185.
[29] N. Jin, Y. Rahmat-Samii, *IEEE Trans. Antennas Propag.* **2007**, *55*, 556.
[30] M. Pu, X. Li, X. Ma, Y. Wang, Z. Zhao, C. Wang, C. Hu, P. Gao, C. Huang, H. Ren, X. Li, F. Qin, J. Yang, M. Gu, M. Hong, X. Luo, *Sci. Adv.* **2015**, *1*, e1500396.
[31] X. Li, L. Chen, Y. Li, X. Zhang, M. Pu, Z. Zhao, X. Ma, Y. Wang, M. Hong, X. Luo, *Sci. Adv.* **2016**, *2*, e1601102.
[32] L. B. Whitbourn, R. C. Compton, *Applied Optics* **1985**, *24*, 217.
[33] K. Huang, H. Ye, J. Teng, P. Yeo Swee, B. Luk'yanchuk, C. W. Qiu, *Laser Photon. Rev.* **2013**, *8*, 152.
[34] X. Luo, T. Ishihara, *Appl. Phys. Lett.* **2004**, *84*, 4780.